Results in Physics 8 (2018) 481–488

Contents lists available at ScienceDirect

Results in Physics

journal homepage: www.journals.elsevier.com/results-in-physics

Endoscopy and homogeneous-heterogeneous reactions in MHD radiative peristaltic activity of Ree-Eyring fluid

Tasawar Hayat [a,b], Javaria Akram [a], Ahmed Alsaedi [b], Hina Zahir [a,*]

[a] Department of Mathematics, Quaid-I-Azam University, 45320 Islamabad 44000, Pakistan
[b] Nonlinear Analysis and Applied Mathematics (NAAM) Research Group, Department of Mathematics, Faculty of Science, King Abdulaziz University, Jeddah 21589, Saudi Arabia

ARTICLE INFO

Article history:
Received 2 November 2017
Received in revised form 5 December 2017
Accepted 20 December 2017
Available online 28 December 2017

Keywords:
Ree-Eyring fluid model
MHD
Endoscope
Homogeneous-heterogeneous reaction
Compliant walls
Slip effects

ABSTRACT

Endoscopic and homogeneous-heterogeneous reactions in MHD peristalsis of Ree-Eyring fluid are addressed. Mathematical modeling and analysis have been performed by utilizing cylindrical coordinates. Nonlinear thermal radiation is present. Impact of slip boundary conditions on temperature and velocity on outer tube are taken into consideration. Lubrication approach is employed. The nonlinear system is executed numerically for solutions of velocity, temperature and concentration. Graphical results are obtained to predict physical interpretation of various embedded parameters. It is noted that homogeneous and heterogeneous reactions affect the concentration alternatively. Moreover Brinkman number rises the temperature and heat transfer coefficient whereas thermal slip drops temperature and heat transfer rate.

Introduction

Non-Newtonian fluids in comparison to viscous materials are more suited in both physiological and industrial processes. Non-Newtonian fluids are used to interpret the properties of complex rheological fluids such as printer inks, blood, grease, polymer solution, paints, lubricants etc. A non-linear relationship between shear stress and shear strain exists for non-Newtonian fluid. Different fluid models have been introduced for investigating non-Newtonian fluids. An influential fluid model for describing shear thinning and thickening effects of non-Newtonian fluids is power law model. However Ree-Eyring fluid model is more suitable than power law model. It can yield a Newtonian fluid for low as well as high shear rates. Moreover its governing equations can be obtained from kinetic theory of fluids rather than empirical solution. Many advancements using non-Newtonian fluid model have been reported by the researchers (see Refs. [1–18]).

Peristaltic activity with magnetohydrodynamics (MHD) is significant in physiology, chemical and industrial procedures. MHD peristaltic flow have found its utilization in MHD compressor operations, power generators, in designs of heat exchangers, blood pump machines, magnetometers, fuel level indicator, radar system and purification of alloys. It also gains much importance in bio-engineering and medical sciences such as cell separation, reducing bleeding during surgeries, hyperthermia, drugs transport and for curing of problems related with gastrointestinal. It acts as working principle of radar system. Some other examples of MHD peristaltic transport of non-Newtonian fluids are purification process of crude oil, nuclear reactors etc. Due to such widespread applications of MHD peristalsis, many researchers have made serious efforts to investigate such flows under different flow conditions. Some works in this direction can be viewed through references [19–29].

Investigations involving chemical reactions have gained continuous considerations from the researchers. Homogeneous-heterogeneous reactions are important in several procedures such as catalysis, fibrous insulation, water and air pollution and fog formation. These reactions are involved in many processes such as combustion and biochemical systems, production of ceramics, distillation processes etc. If a reaction takes place on single phase then it is known as homogeneous reaction whereas a heterogeneous reaction occurs in more than one phases. Homogeneous reactions are quite simpler than heterogeneous reaction since the product of homogeneous reactions are characterized by properties of reacting materials. Few applications of heat and mass transfer via chemical reactions are observed in hydro-metallurgical devices, batteries, food processing, fog formation and production of polymers. Such reactions are boosted by a catalyst to approach the desired limit of reaction. Some efforts on investigating the effects

* Corresponding author.
E-mail address: hinazahir@math.qau.edu.pk (H. Zahir).

https://doi.org/10.1016/j.rinp.2017.12.056
2211-3797/

of homogeneous-heterogeneous reactions in peristalsis are made by the researchers (see [30–36]).

To our view, no attempt discussing endoscopic relevance in MHD peristaltic transport of Ree-Eyring fluid under impact of homogeneous and heterogeneous reactions yet exists. Flexible property of boundary is considered. Slip conditions for velocity and temperature are accounted. The system of equations governing flow, heat and mass transfer is formulated in cylindrical coordinates and reduced under the long wavelength and low Reynolds number assumption. Numerical technique for solution of velocity, temperature and concentration is employed. Physical interpretation of different pertinent parameters on physical quantities is presented. It is noticed that velocity decrease in view of larger Hartman number. The slip parameter on velocity has similar observation. Temperature is found to decrease by Prandtl number. Temperature is further decayed by thermal slip. Thermal layer thickness is decreasing function of Prandtl number. Schmidt number decays the concentration. Homogenous reaction has same influence qualitatively when compared with Schmidt number. Heat transfer coefficient has similar effect for Prandtl number and radiation parameter.

Formulation

MHD peristaltic flow of incompressible Ree-Eyring fluid is considered. It has been assumed that inner tube is fixed while sinusoidal waves with constant velocity c propagates along outer tube (see Fig. 1). The walls of tubes are considered flexible. Viscous dissipation is present. Impact of homogeneous-heterogeneous reaction is also retained here.

The equations for geometry of wall surface are expressed as

$$\bar{r}_1 = \acute{a}_1, \tag{1}$$

$$\bar{r}_2 = \acute{a}_2 + \acute{b}\sin\left\{\frac{2\pi}{\lambda}(\bar{z} - c\bar{t})\right\}. \tag{2}$$

Here $\acute{a}_1$ and $\acute{a}_2$ denote the radii of inner and outer tubes respectively. Moreover peristaltic wave have amplitude $\acute{b}$ and wavelength λ. Velocity field is

$$\overline{\mathbf{V}} = [\bar{u}(\bar{r},\bar{z},\bar{t}), 0, \bar{w}(\bar{r},\bar{z},\bar{t})].$$

where $\bar{r}$-*axis* represents radial direction and $\bar{z}$-*axis* along the center line of tubes. Radial applied magnetic field with strength B_0 is

$$\mathbf{B} = (B_0, 0, 0). \tag{3}$$

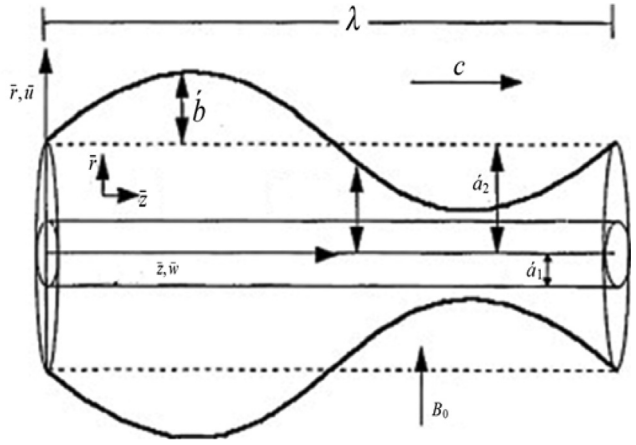

Fig. 1. Flow geometry.

By Ohm's law one has

$$\mathbf{J} = \sigma(\overline{\mathbf{E}} + \overline{\mathbf{V}} \times \mathbf{B}), \tag{4}$$

Here impact of electric field is assumed absent i.e. $\overline{\mathbf{E}} = \mathbf{0}$ and thus

$$\mathbf{J} \times \mathbf{B} = \left(0, 0, -\sigma B_0^2 \bar{w}\right), \tag{5}$$

where σ denotes electric conductivity of fluid and $\mathbf{J}$ the current density.

The homogeneous-heterogeneous reaction is mathematically modeled as

$$\overline{A} + 2\overline{B} \to 3\overline{B}, \quad \text{rate} = K_c \acute{a}\acute{b}^2.$$

On catalyst surface, a single, first order and isothermal reaction retains the form

$$\overline{A} \to \overline{B}, \quad \text{rate} = K_s \acute{a}.$$

Both reactions occur at same temperature and rate constants symbolized by K_c and K_s.

The expressions for flow under consideration are [36,37]

$$\frac{\partial \bar{u}}{\partial \bar{r}} + \frac{\bar{u}}{\bar{r}} + \frac{\partial \bar{w}}{\partial \bar{z}} = 0, \tag{6}$$

$$\rho\left[\frac{\partial \bar{u}}{\partial \bar{t}} + \bar{u}\frac{\partial \bar{u}}{\partial \bar{r}} + \bar{w}\frac{\partial \bar{u}}{\partial \bar{z}}\right] = -\frac{\partial \bar{p}}{\partial \bar{r}} + \frac{1}{\bar{r}}\frac{\partial}{\partial \bar{r}}(\bar{r}\bar{S}_{\bar{r}\bar{r}}) + \frac{\partial}{\partial \bar{z}}(\bar{S}_{\bar{r}\bar{z}}) - \frac{\bar{S}_{\bar{\theta}\bar{\theta}}}{\bar{r}}, \tag{7}$$

$$\rho\left[\frac{\partial \bar{w}}{\partial \bar{t}} + \bar{u}\frac{\partial \bar{w}}{\partial \bar{r}} + \bar{w}\frac{\partial \bar{w}}{\partial \bar{z}}\right] = -\frac{\partial \bar{p}}{\partial \bar{z}} + \frac{1}{\bar{r}}\frac{\partial}{\partial \bar{r}}(\bar{r}\bar{S}_{\bar{r}\bar{z}}) + \frac{\partial}{\partial \bar{z}}(\bar{S}_{\bar{z}\bar{z}}) - \sigma B_0^2 \bar{w}, \tag{8}$$

$$\rho c_p\left[\frac{\partial \acute{T}}{\partial \bar{t}} + \bar{u}\frac{\partial \acute{T}}{\partial \bar{r}} + \bar{w}\frac{\partial \acute{T}}{\partial \bar{z}}\right] = k\left[\frac{\partial^2 \acute{T}}{\partial \bar{r}^2} + \frac{1}{\bar{r}}\frac{\partial \acute{T}}{\partial \bar{r}} + \frac{\partial^2 \acute{T}}{\partial \bar{z}^2}\right] - \frac{\partial q_r}{\partial \bar{r}} + \left[\bar{S}_{\bar{r}\bar{r}}\frac{\partial \bar{u}}{\partial \bar{r}} + \bar{S}_{\bar{r}\bar{z}}\frac{\partial \bar{w}}{\partial \bar{r}} + \bar{S}_{\bar{r}\bar{z}}\frac{\partial \bar{u}}{\partial \bar{z}} + \bar{S}_{\bar{z}\bar{z}}\frac{\partial \bar{w}}{\partial \bar{z}}\right], \tag{9}$$

$$\frac{d\hat{a}}{d\bar{t}} = D_{\overline{A}}\nabla^2 \hat{a} - K_c \hat{a}\hat{b}^2, \tag{10}$$

$$\frac{d\hat{b}}{d\bar{t}} = D_{\overline{B}}\nabla^2 \hat{b} + K_c \hat{a}\hat{b}^2. \tag{11}$$

In view of Rosseland approximation, nonlinear radiative heat flux q_r can be written as

$$q_r = -\frac{16\hat{\sigma}}{3\hat{k}}\acute{T}^3\frac{\partial \acute{T}}{\partial \bar{r}}. \tag{12}$$

Here $\hat{\sigma}$ defines Stefan–Boltzmann constant and $\hat{k}$ the coefficient of mean absorption. In above relations ρ specifies the fluid density, k the thermal conductivity, c_p the specific heat coefficient and $D_{\overline{A}}$ and $D_{\overline{B}}$ the diffusion coefficients for homogeneous and heterogeneous reactions respectively. Moreover temperature of fluid is denoted by T and $\hat{a}$ and $\hat{b}$ depict the concentrations for homogeneous and heterogeneous reactions respectively. $\bar{S}_{\bar{r}\bar{r}}, \bar{S}_{\bar{r}\bar{z}}, \bar{S}_{\bar{z}\bar{z}}$ are extra stress components of Ree-Eyring stress tensor $\overline{\mathbf{S}}$ expressed by

$$\overline{\mathbf{S}} = \left[\mu \text{grad}(\overline{\mathbf{V}}) + \frac{1}{B}\sinh^{-1}\left(\frac{\text{grad}(\overline{\mathbf{V}})}{C}\right)\right],$$
$$\mathbf{L} = \text{grad}(\overline{\mathbf{V}}), \tag{13}$$

in which B and C are the material constants and μ the fluid dynamic viscosity.

The related conditions are

$$\bar{w} = 0,\ \acute{T} = T_0 \text{ at } \bar{r} = \bar{r}_1, \tag{14}$$

$$\bar{w} - \beta_1^* \bar{S}_{\bar{r}\bar{z}} = 0,\ \acute{T} - \beta_2^* \frac{\partial \acute{T}}{\partial \bar{r}} = T_1 \text{ at } \bar{r} = \bar{r}_2, \tag{15}$$

$$\left[-\acute{\tau}\frac{\partial^3}{\partial \bar{z}^3} + \acute{m}_1 \frac{\partial^3}{\partial \bar{z}\partial \bar{t}^2} + d' \frac{\partial^2}{\partial \bar{z}\partial \bar{t}}\right]\bar{r}_2 = -\rho_f \left[\frac{\partial \bar{w}}{\partial \bar{t}} + \bar{u}\frac{\partial \bar{w}}{\partial \bar{r}} + \bar{w}\frac{\partial \bar{w}}{\partial \bar{z}}\right] + \frac{1}{\bar{r}}\frac{\partial}{\partial \bar{r}}(\bar{r}\bar{S}_{\bar{r}\bar{z}}) + \frac{\partial}{\partial \bar{z}}(\bar{S}_{\bar{z}\bar{z}}) - \sigma B_0^2 \bar{w} \text{ at } \bar{r} = \bar{r}_1,\ \bar{r}_2, \tag{16}$$

$$\hat{a} \to \hat{a}_0,\ \hat{b} \to 0 \text{ at } \bar{r} = \bar{r}_1, \tag{17}$$

$$D_{\bar{A}}\frac{\partial \hat{a}}{\partial \bar{r}} - K_s \hat{a} = 0,\ D_{\bar{B}}\frac{\partial \hat{b}}{\partial \bar{r}} + K_s \hat{b} = 0 \text{ at } \bar{r} = \bar{r}_2 \tag{18}$$

in which T_0 and T_1 are the temperatures maintained at inner and outer tubes, β_1^* the velocity slip parameter, β_2^* the temperature slip parameter, $\acute{\tau}, \acute{m}_1$ and d' signify coefficients of elastic tension, viscous damping and mass per unit area respectively.

Defining variables

$$r = \frac{\bar{r}}{a_2},\ z = \frac{\bar{z}}{\lambda},\ w = \frac{\bar{w}}{c},\ t = \frac{c\bar{t}}{\lambda},\ u = \frac{\lambda}{a_2 c}\bar{u},\ p = \frac{a_2^2 \bar{p}}{\mu c \lambda},$$

$$\delta = \frac{a_2}{\lambda},\ \mathrm{Pr} = \frac{\mu c_p}{k},\ Sc = \frac{\mu}{\rho D_{\bar{A}}},$$

$$r_1 = \frac{\bar{r}_1}{\acute{a}_2} = \frac{\acute{a}_1}{\acute{a}_2} = \epsilon,\ r_2 = \frac{\bar{r}_2}{\acute{a}_2} = 1 + \phi \sin 2\pi(z - t),$$

$$\mathrm{Re} = \frac{\rho c \acute{a}_2}{\mu},\ \mathbf{S} = \frac{\acute{a}_2 \bar{\mathbf{S}}}{\mu c},\ \theta = \frac{\acute{T} - \acute{T}_1}{\acute{T}_0 - \acute{T}_1},$$

$$\beta_1 = \frac{\beta_1^*}{\acute{a}_2},\ \beta_2 = \frac{\beta_2^*}{\acute{a}_2},\ H^2 = \frac{\sigma B_0^2 \acute{a}_2^2}{\mu},\ E_1 = -\frac{\tau_1 d_1^3}{\lambda^3 \mu c},$$

$$E_2 = \frac{m_1 c d_1^3}{\mu \lambda^3},\ E_3 = \frac{d_1^3 d'}{\mu \lambda^2},$$

$$Br = Ec\,\mathrm{Pr},\ E_c = \frac{c^2}{c_p(\acute{T}_0 - \acute{T}_1)},\ Rd = \frac{16\hat{\sigma}}{3\hat{k}\mu c_p}\acute{T}_1^3,\ a = \frac{\hat{a}}{a_0},$$

$$b = \frac{\hat{b}}{a_0},\ K = \frac{K_c \rho a_0^2 \acute{a}_2^2}{\mu},$$

$$M = \frac{K_s \acute{a}_2}{D_{\bar{A}}},\ \alpha = \frac{1}{\mu BC},\ \theta_w = \frac{T_0}{T_1}. \tag{19}$$

Eqs. (6)–(11) give

$$\frac{\partial u}{\partial r} + \frac{u}{r} + \frac{\partial w}{\partial z} = 0, \tag{20}$$

$$\mathrm{Re}\,\delta^3\left[\frac{\partial u}{\partial t} + u\frac{\partial u}{\partial r} + w\frac{\partial u}{\partial z}\right] = -\frac{\partial p}{\partial r} + \frac{\delta}{r}\frac{\partial}{\partial r}(rS_{rr}) + \delta^2\frac{\partial S_{rz}}{\partial z} - \delta\frac{S_{\theta\theta}}{r}, \tag{21}$$

$$\mathrm{Re}\,\delta\left[\frac{\partial w}{\partial t} + u\frac{\partial w}{\partial r} + w\frac{\partial w}{\partial z}\right] = -\frac{\partial p}{\partial z} + \frac{1}{r}\frac{\partial}{\partial r}(rS_{rz}) + \delta\frac{\partial S_{zz}}{\partial z} - H^2 w, \tag{22}$$

$$\mathrm{PrRe}\,\delta\left[\frac{\partial \theta}{\partial t} + u\frac{\partial \theta}{\partial r} + w\frac{\partial \theta}{\partial z}\right] = \left[\frac{\partial^2 \theta}{\partial r^2} + \frac{1}{r}\frac{\partial \theta}{\partial r} + \delta^2\frac{\partial^2 \theta}{\partial z^2}\right] + \mathrm{PrRd}\left(3(\theta(\theta_w - 1) + 1)^2(\theta_w - 1)\left(\frac{\partial \theta}{\partial y}\right)^2 + (\theta(\theta_w - 1) + 1)^3\frac{\partial^2 \theta}{\partial y^2}\right) + \mathrm{PrEc}\left[\delta S_{rr}\frac{\partial u}{\partial r} + S_{rz}\frac{\partial w}{\partial r} + \delta^2 S_{rz}\frac{\partial u}{\partial z} + \delta S_{zz}\frac{\partial w}{\partial z}\right], \tag{23}$$

$$\mathrm{Re}\,\delta\left[\frac{\partial a}{\partial t} + u\frac{\partial a}{\partial r} + w\frac{\partial a}{\partial z}\right] = \frac{1}{Sc}\left[\frac{\partial^2 a}{\partial r^2} + \frac{1}{r}\frac{\partial a}{\partial r} + \delta^2\frac{\partial^2 a}{\partial z^2}\right] + Kab^2, \tag{24}$$

$$\mathrm{Re}\,\delta\left[\frac{\partial b}{\partial t} + u\frac{\partial b}{\partial r} + w\frac{\partial b}{\partial z}\right] = \frac{1}{Sc}\left[\frac{\partial^2 b}{\partial r^2} + \frac{1}{r}\frac{\partial b}{\partial r} + \delta^2\frac{\partial^2 b}{\partial z^2}\right] - Kab^2. \tag{25}$$

$$S_{rr} = \delta(1 + \alpha)\frac{\partial u}{\partial r}, \tag{26}$$

$$S_{rz} = (1 + \alpha)\frac{\partial w}{\partial r}, \tag{27}$$

$$S_{zz} = \delta(1 + \alpha)\frac{\partial w}{\partial z}. \tag{28}$$

In above equations, δ denotes the wave number, Rd the radiation parameter, Re the Reynolds number, K and M are the parameters measuring the strength of homogeneous and heterogeneous reaction respectively, Pr the Prandtl number, θ_w the temperature ratio parameter, Ec the Eckert number, H the Hartman number, Br the Brinkman number and Sc the Schmidt number.

Introducing non-dimensional stream function in terms of velocity components

$$u = -\frac{1}{r}\frac{\partial \psi}{\partial z}, \qquad w = \frac{1}{r}\frac{\partial \psi}{\partial r}. \tag{29}$$

and then using large wavelength and small Reynolds number one obtains

$$\frac{\partial p}{\partial r} = 0, \tag{30}$$

$$\frac{\partial p}{\partial z} - \frac{1}{r}\frac{\partial}{\partial r}(rS_{rz}) - H^2\left(\frac{1}{r}\frac{\partial \psi}{\partial r}\right) = 0, \tag{31}$$

$$\frac{\partial^2 \theta}{\partial r^2} + \frac{1}{r}\frac{\partial \theta}{\partial r} + \mathrm{PrRd}\left(3(\theta(\theta_w - 1) + 1)^2(\theta_w - 1)\left(\frac{\partial \theta}{\partial y}\right)^2 + (\theta(\theta_w - 1) + 1)^3\frac{\partial^2 \theta}{\partial y^2}\right) + BrS_{rz}\left(\frac{1}{r}\frac{\partial^2 \psi}{\partial r^2} - \frac{1}{r^2}\frac{\partial \psi}{\partial r}\right) = 0, \tag{32}$$

$$\frac{\partial^2 a}{\partial r^2} + \frac{1}{r}\frac{\partial a}{\partial r} + ScKab^2 = 0, \tag{33}$$

$$\xi\left(\frac{\partial^2 b}{\partial r^2} + \frac{1}{r}\frac{\partial b}{\partial r}\right) - ScKab^2 = 0. \tag{34}$$

$$S_{rr} = 0, \tag{35}$$

$$S_{rz} = (1 + \alpha)\left(\frac{1}{r}\frac{\partial^2 \psi}{\partial r^2} - \frac{1}{r^2}\frac{\partial \psi}{\partial r}\right) \tag{36}$$

$$S_{zz} = 0, \tag{37}$$

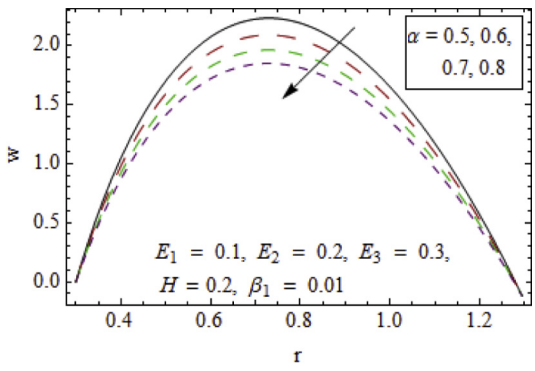

Figs. 2–5. Velocity field w when $\epsilon = 0.3, z = 0.2$ and $t = 0.1$.

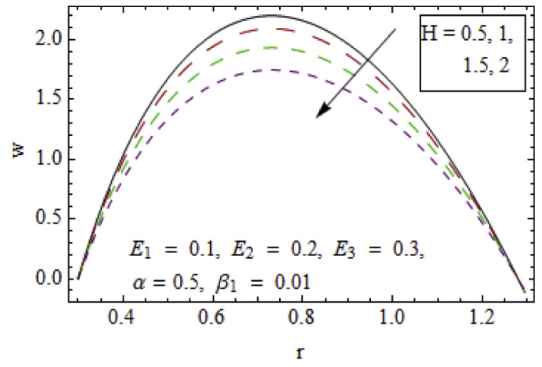

Fig. 3

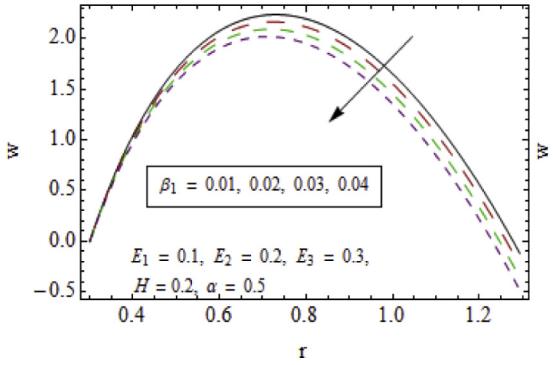

Fig. 4

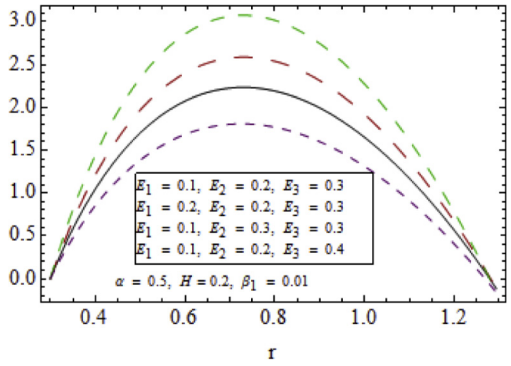

Fig. 5

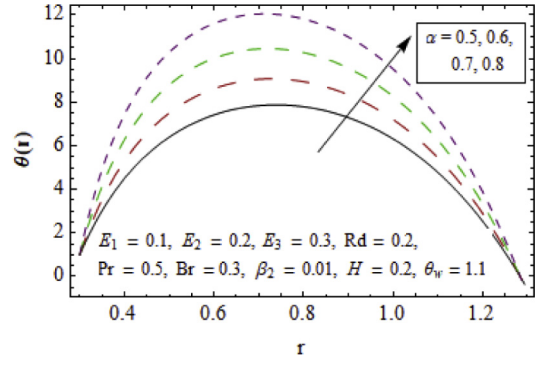

Figs. 6–13. Temperature $\theta(r)$ when $\epsilon = 0.3, z = 0.2$ and $t = 0.1$.

with α denoting Ree-Eyring fluid parameter and incompressibility condition is trivially satisfied. After eliminating pressure from Eqs. (30) and (31) we get

$$\frac{\partial}{\partial r}\left(\frac{1}{r}\frac{\partial}{\partial r}(rS_{rz})\right) - H^2\left(\frac{1}{r}\frac{\partial^2\psi}{\partial r^2} - \frac{1}{r^2}\frac{\partial\psi}{\partial r}\right) = 0, \tag{38}$$

The dimensionless boundary conditions are

$$\frac{\partial\psi}{\partial r} = 0 \text{ at } r = r_1, \tag{39}$$

$$\frac{1}{r}\frac{\partial\psi}{\partial r} - \beta_1(1+\alpha)\left(\frac{1}{r}\frac{\partial^2\psi}{\partial r^2} - \frac{1}{r^2}\frac{\partial\psi}{\partial r}\right) = 0 \text{ at } r = r_2, \tag{40}$$

$$\theta = 1 \text{ at } r = r_1,\ \theta - \beta_2\frac{\partial\theta}{\partial r} = 0 \text{ at } r = r_2, \tag{41}$$

$$E_1\frac{\partial^3 r_2}{\partial z^3} + E_2\frac{\partial^3 r_2}{\partial z\partial t^2} + E_3\frac{\partial^2 r_2}{\partial z\partial t} = \frac{1}{r}\frac{\partial}{\partial r}(rS_{rz}) - H^2\left(\frac{1}{r}\frac{\partial\psi}{\partial r}\right) \text{ at } r = r_1, r_2. \tag{42}$$

$$a = 1 \text{ at } r = r_1, \frac{\partial a}{\partial r} - Ma = 0 \text{ at } r = r_2, \tag{43}$$

$$b = 0 \text{ at } r = r_1, \xi\frac{\partial b}{\partial r} + Mb = 0 \text{ at } r = r_2. \tag{44}$$

In above expressions β_1 and β_2 represent velocity and thermal slip parameters respectively, E_1 the wall tension parameter, E_2 the wall mass parameter and E_3 the wall damping parameter.

The diffusion coefficients $D_{\overline{A}}$ and $D_{\overline{B}}$ of chemical species $\overline{A}$ and $\overline{B}$ are assumed equal in size. Hence $\xi = 1$ leads to

$$a + b = 1. \tag{45}$$

Using above relation, the resulting concentration equation and corresponding boundary conditions are

$$\frac{\partial^2 a}{\partial r^2} + \frac{1}{r}\frac{\partial a}{\partial r} + ScKa(1-a)^2 = 0, \tag{46}$$

$$a = 1 \text{ at } r = r_1,\ \frac{\partial a}{\partial r} - Ma = 0 \text{ at } r = r_2, \tag{47}$$

Heat transfer coefficient at outer tube walls can be computed through temperature involvement by mathematical expression as

$$Z = \frac{\partial r_2}{\partial z}\left|\frac{\partial\theta}{\partial r}\right|_{r\to r_2}. \tag{48}$$

Solution procedure and discussion

The solution of non-linear coupled system of equations is evaluated numerically through built-in routine of Mathematica. Such numerical technique is beneficial in minimizing the error and reducing CPU time per evaluation. It chooses an appropriate algorithm for solving the problem. Moreover complicated form of solutions can be avoided in this technique and graphical results can be obtained directly. The graphical descriptions of axial velocity w, temperature θ concentration a and heat transfer coefficient Z for emerging physical parameters such as Hartman number H, fluid parameter α, wall parameters $E_i (i = 1, 2, 3)$, slip parameters β_1 and β_2, Schmidt number Sc, radiation parameter Rd, Brinkman number Br, temperature ratio parameter θ_w, Prandtl number Pr and strength parameters for homogeneous and heterogeneous reactions i.e. K and M respectively are discussed.

Velocity

Physical description of velocity field for different involved parameters is illustrated in this subsection. Decaying behavior of velocity for fluid parameter α can be seen through Fig. 2. Decreasing response of velocity for magnetic field is witnessed through

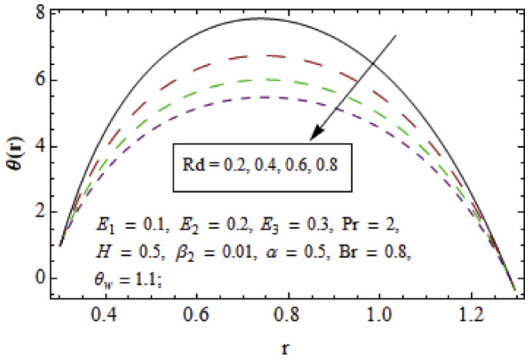

Fig. 7

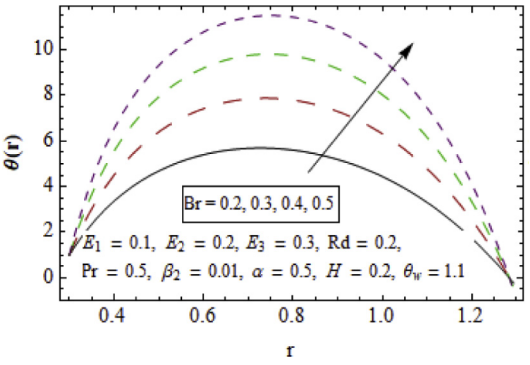

Fig. 8

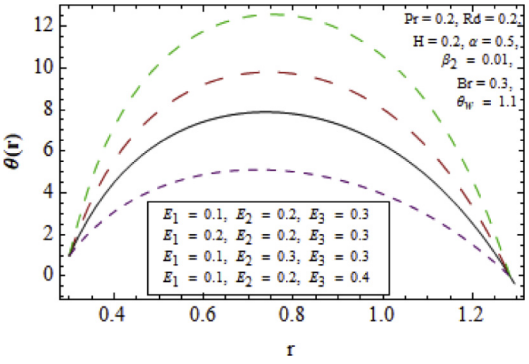

Fig. 9

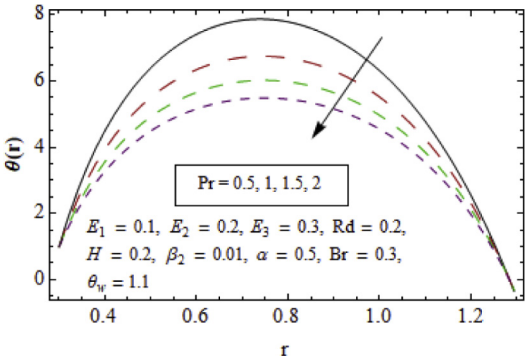

Fig. 10

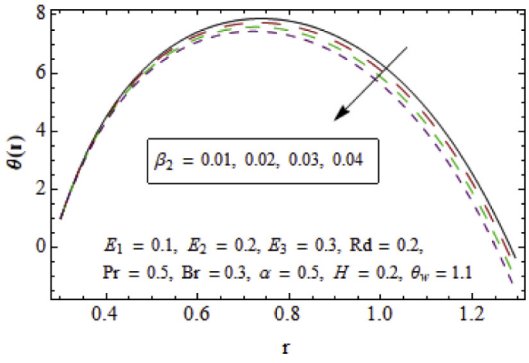

Fig. 11

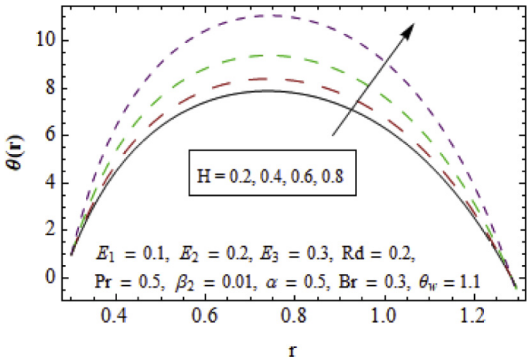

Fig. 12

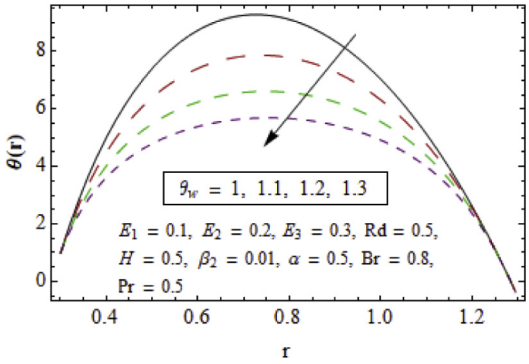

Fig. 13

Fig. 3 Since radial magnetic field causes resistance to flow of fluid therefore for larger Hartman number H the resistive forces become stronger. Hence velocity declines. Fig. 4 is plotted for impact of β_1 on velocity field. The displayed graph manifests that velocity declines for larger slip parameter. Physically for larger slip parameter fluid is less affected by motion of boundary. As a result the velocity decreases. Impression of wall parameters E_1, E_2 and E_3 on velocity is explored in Fig. 5. Resulting graph shows an increment in velocity for larger elasticity parameter E_1 and wall mass E_2. Physically less resistance is experienced by fluid from flexible walls as elasticity increases which corresponds to higher velocity. However velocity decreases upon increasing E_3 because damping force generates more resistance to flow.

Temperature

Temperature for physical parameter is analyzed through Figs. 6–13. Fig. 6 is plotted for the response of temperature towards larger

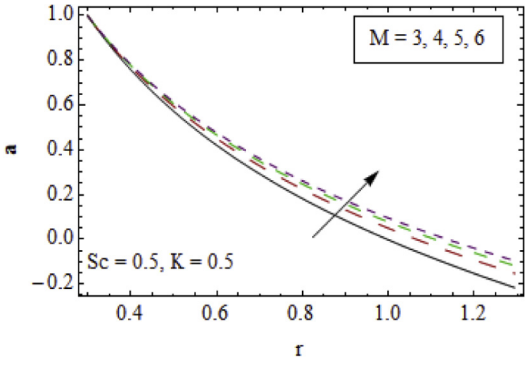

Figs. 14–16. Concentration when $\epsilon = 0.3, z = 0.2$ and $t = 0.1$.

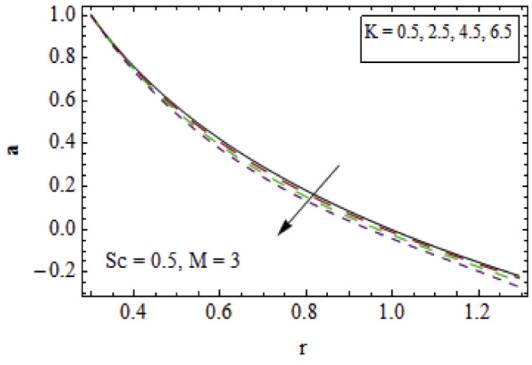

Fig. 15

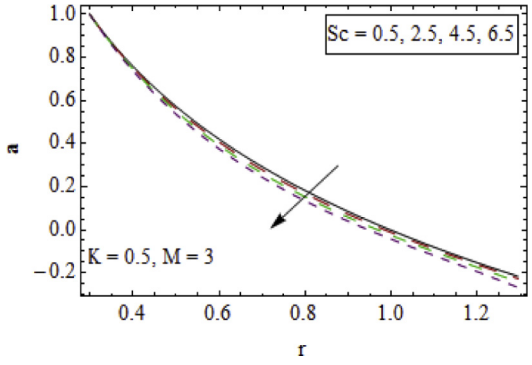

Fig. 16

Ree-Eyring fluid parameter α. Increasing response of α towards temperature is noticed. It is due to decrease in viscosity of fluid. In Fig. 7 temperature is plotted against radiation parameter *Rd*. Decaying behavior of temperature is examined for higher values of *Rd*. Since less amount of energy is absorbed by fluid for stronger radiation effect therefore temperature decreases. A reinforcement in θ is observed for rising values of Brinkman number through Fig. 8. It is because of the fact that for larger *Br* more friction is experienced by fluid and temperature grows. Fig. 9 captured the outcomes of wall parameters on temperature. Temperature dominates for rise in elasticity E_1 and mass parameter E_2 whereas decaying behavior is exhibited by temperature for damping parameter E_3. As temperature and velocity are directly related to each other by virtue of kinetic energy therefore similar impact of wall parameter on temperature and velocity is achieved. This impact of wall parameters on θ is well matched with Hayat et al. [31]. It can be visualized from Fig. 10 that Prandtl number has inverse relation with temperature. There is reduction in boundary layer thickness of fluid for larger Pr. Obtained influence of Prandtl number on temperature profile has great relevance with Hayat et al. [33]. Temperature slip parameter β_2 has a reverse impact on θ (see Fig. 11). This result is in great accordance with study of Maryiam et al. [35]. Effect of Hartman number *H* on temperature is portrayed in Fig. 12. A significant rise in temperature appears in resulting sketch. Since Lorentz forces obstruct the flow of fluid therefore more heat is generated and thermal boundary layer becomes thicker. This result of *H* on temperature is compatible with Hayat et al. [38]. Fig. 13 provides an analysis for impact of temperature ratio parameter on thermal field. It is revealed that reduction occurred in temperature profile for larger values of θ_w. For $\theta_w = 1$, the results of linear radiative heat transfer case are recovered.

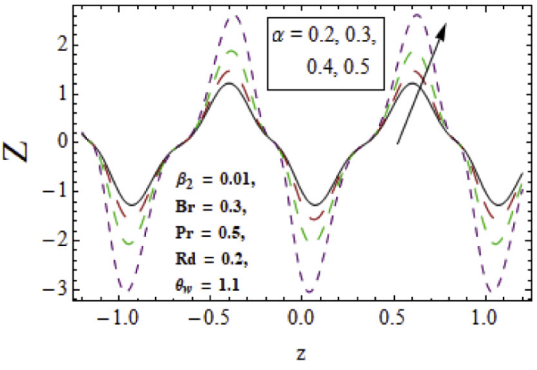

Figs. 17–22. Heat transfer coefficient *Z* when $\epsilon = 0.3$ and $t = 0.1$.

Homogeneous-heterogeneous reactions effects

Consequences of different influential parameters on concentration are illustrated in this portion. Inner tube is fixed so graphical interpretation is studied at outer tube. Fig. 14 demonstrates the change in concentration for variation in heterogeneous reaction parameter *M*. The concentration of species rises for larger *M*. Similar impact of heterogeneous reaction parameter *M* is reported by Anum et al. [36]. Concentration rapidly decreases for larger values of homogeneous reaction parameter *K* (see Fig. 15). It is due to reduction in kinematic viscosity of fluid for stronger homogeneous reaction. Decrease in concentration is captured when plotted against Schmidt number *Sc* (see Fig. 16). It is noteworthy that larger Schmidt number comprise reduction in molecular diffusion which in turn decays concentration.

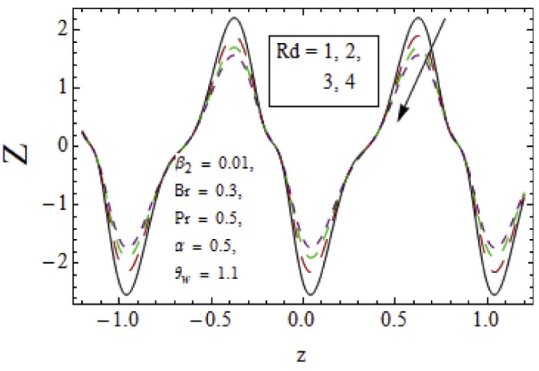

Fig. 18

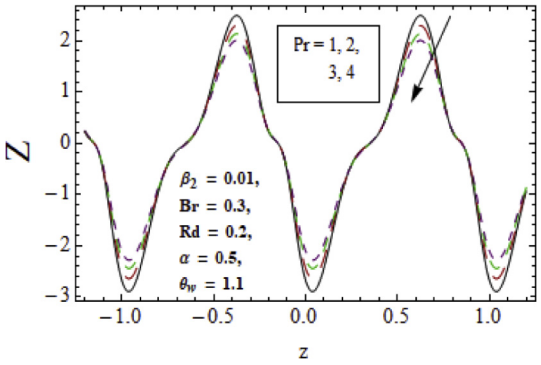

Fig. 19

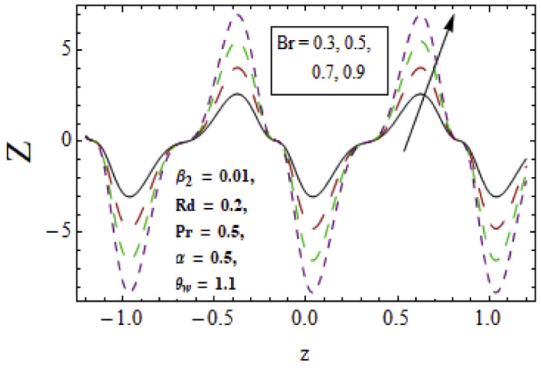

Fig. 20

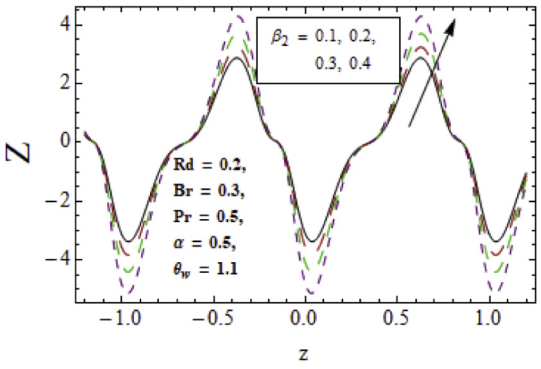

Fig. 21

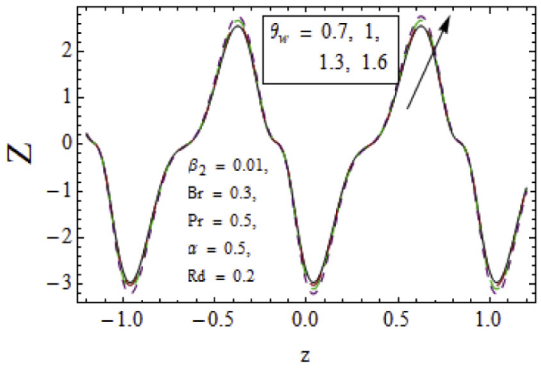

Fig. 22

Heat transfer coefficient

Figs. 17–22 are plotted to visualize heat transfer coefficient for variation in different embedded parameters. Fig. 17 illustrates behavior of heat transfer coefficient towards fluid parameter α. Heat transfer coefficient grows for an increment in α. Infact resistive forces dominate for higher α which tend to rise the magnitude of heat transfer coefficient. Fig. 18 portrays the influence of radiation parameter *Rd* on heat transfer coefficient. Fig. 18 ensures that by increasing radiation parameter the heat transfer rate is reduced. Similar impact of radiation parameter is obtained by Hayat et al. [39]. A decaying impact of Prandtl number Pr on *Z* is elucidated by Fig. 19. For larger Prandtl number there is a reduction in thermal diffusitivity and magnitude of heat transfer decays. Heat transfer coefficient is intensified for multiple values of Brinkman number *Br* as depicted in Fig. 20. With the strength of viscous dissipative forces the heat transfer rate dominates due to collision between fluid particles. The process of heat transfer decayed upon increasing values of temperature slip parameter (see Fig. 21). This observation is similar to that of Hayat et al. [40]. Fig. 22 highlights the variation in heat transfer rate for temperature ratio parameter. It is evident that thermal boundary layer thickness grows due to larger temperature difference between tube walls for rise in θ_w which corresponds to higher rate of heat transfer.

Concluding remarks

Investigation of endoscope on MHD peristaltic transport of Ree-Eyring fluid with magnetic field, homogeneous-heterogeneous reactions, viscous dissipation and nonlinear thermal radiation is carried out. Some findings of this study are listed below.

- Temperature and heat transfer coefficient exhibit more response towards fluid parameter α whereas opposite behavior is shown by velocity profile for α.
- Slip and wall parameters affect velocity and temperature in similar manner.
- Larger magnetic field decays fluid velocity.
- Larger radiation parameter *Rd* tend to decline both temperature and heat transfer coefficient.
- Temperature enhances via Brinkman number. However Prandtl number has decreasing impact on temperature.
- Temperature of fluid is intensified for magnetic field.
- Dominant behavior is exhibited by concentration of fluid for stronger heterogeneous reaction parameter *M* but it reduces for larger homogeneous reaction.
- Concentration is decreased by Schmidt number.
- Impression of temperature ratio parameter on heat transfer coefficient is more whereas opposite impact is noticed for temperature profile.
- Prandtl Pr and Brinkman numbers *Br* have reverse impact on heat transfer coefficient.

References

[1] Hayat T, Muhammad T, Ahmad B, Shehzad SA. Impact of magnetic field in three-dimensional flow of Sisko nanofluid with convective condition. J Magn Magn Mater 2016;413:1–8.
[2] Feng S, Chen Q. Analysis on non-Newtonian characteristics for nano magnetic fluid. Pro Eng 2017;174:1208–14.
[3] Krishna PM, Sandeep N, Reddy JVR, Sugunamma V. Dual solutions for unsteady flow of Powell-Eyring fluid past an inclined stretching sheet. J Naval Arch Marine Eng 2016;13:89–99.
[4] Abegunrin OA, Animasaun IL, Sandeep N. Insight into the boundary layer flow of non-Newtonian Eyring-Powell fluid due to catalytic surface reaction on an upper horizontal surface of a paraboloid of revolution. Alex Eng J 2017. https://doi.org/10.1016/j.aej.2017.05.018.

[5] Hayat T, Shehzad SA, Alsaedi A. Soret and Dufour effects on magnetohydrodynamic (MHD) flow of Casson fluid. Appl Math Mech 2012;33:1301–12.
[6] Nithyadevi N, Gayathri P, Sandeep N. Boundary stratum exploration of unsteady 3D MHD stagnation point flow of Al–Cu water nanofluid. Int J Mech Sci 2017;131–132:827–35.
[7] Hayat T, Zahir H, Alsaedi A, Ahmad B. Heat transfer analysis on peristaltic transport of Ree-Eyring fluid in rotating frame. Chin J Phys 2017;55:1894–907.
[8] Hayat T, Shehzad SA, Qasim M, Obaidat S. Radiative flow of Jeffery fluid in a porous medium with power law heat flux and heat source. Nucl Eng Des 2012;243:15–9.
[9] Khan M, Maqbool K, Hayat T. Influence of Hall current on the f lows of a generalized Oldroyd-B f luid in a porous space. Acta Mech 2006;184:1–13.
[10] Hayat T, Imtiaz M, Alsaedi A, Kutbi MA. MHD three-dimensional flow of nanofluid with velocity slip and nonlinear thermal radiation. J Magn Magn Mater 2015;396:31–7.
[11] Hayat T, Qasim M, Mesloub S. MHD flow and heat transfer over permeable stretching sheetwith slip conditions. Int J Numer Meth Fluids 2011;66:963–75.
[12] Hayat T, Ahmed Naveed, Sajid M, Asghar S. On the MHD flow of a second grade fluid in a porous channel. Comp Math Appl 2007;54:407–14.
[13] Ramzan M, Bilal M, Kanwal S, Chung JD. Effects of variable thermal conductivity and non-linear thermal radiation past an eyring powell nanofluid flow with chemical reaction. Commun Theor Phys 2017;67.
[14] Ramzan M, Bilal M, Chung JD, Mann AB. On MHD radiative Jeffery nanofluid flow with convective heat and mass boundary conditions. Neural Comput Appl 2017. https://doi.org/10.1007/s00521-017-2852-8.
[15] Ramzan M, Bilal M, Chung JD. Effects of MHD homogeneous-heterogeneous reactions on third grade fluid flow with Cattaneo-Christov heat flux. J Mol Liq 2016;223:1284–90.
[16] Ramzan M, Bilal M, Chung JD. Effects of thermal and solutal stratification on jeffrey magneto-nanofluid along an inclined stretching cylinder with thermal radiation and heat generation/absorption. Int J Mech Sci 2017;131–132:317–24.
[17] Ramzan M, Bilal M, Chung JD. MHD stagnation point Cattaneo-Christov heat flux in Williamson fluid flow with homogeneous–heterogeneous reactions and convective boundary condition — A numerical approach. J Mol Liq 2017;225:856–62.
[18] Sandeep N. Effect of aligned magnetic field on liquid thin film flow of magnetic-nanofluid embedded with graphene nanoparticles. Adv Powder Technol 2017;28:865–75.
[19] Abd-Alla AM, Abo-Dahab SM, Kilicman A. Peristaltic flow of a Jeffrey fluid under the effect of radially varying magnetic field in a tube with an endoscope. J Magn Magn Mater 2015;348:79–86.
[20] Hayat T, Tanveer A, Alsaadi F, Mousa G. Impact of radial magnetic field on peristalsis in curved channel with convective boundary conditions. J Magn Magn Mater 2016;403:47–59.
[21] Reddy MG, Makinde OD. Magnetohydrodynamic peristaltic transport of Jeffrey nanofluid in an asymmetric channel. J Mol Liq 2016;223:1242–8.
[22] Abbasi FM, Hayat T, Alsaedi A. Numerical analysis for MHD peristaltic transport of Carreau-Yasuda fluid in a curved channel with Hall effects. J Magn Magn Mater 2015;382:104–10.
[23] Hayat T, Zahir H, Tanveer A, Alsaedi A. Numerical study for MHD peristaltic flow in a rotating frame. Comp Bio Med 2016;79:215–21.
[24] Abd-Alla AM, Abo-Dahab SM. Magnetic field and rotation effects on peristaltic transport of a Jeffrey fluid in an asymmetric channel. J Magn Mag Mater 2015;374:680–9.
[25] Hayat T, Bibi S, Rafiq M, Alsaedi A, Abbasi FM. Effects of an inclined magnetic field on peristaltic flow of Williamson fluid in an inclined channel with convective conditions. J Magn Mag Mater 2016;401:733–45.
[26] Reddy MG. Heat and mass transfer on magnetohydrodynamic peristaltic flow in a porous medium with partial slip. Alex Eng J 2016;55:1225–34.
[27] Latif T, Alvi N, Hussain Q, Asghar S. Variable properties of MHD third order fluid with peristalsis. Res Phy 2016;6:963–72.
[28] Hayat T, Aslam N, Alsaedi A, Rafiq M. Numerical study for MHD peristaltic transport of Sisko nanofluid in a curved channel. Int J Heat Mass Transfer 2017;109:1281–8.
[29] Bhatti MM, Zeeshan A, Ellahi R. Endoscope analysis on peristaltic blood flow of Sisko fluid with Titanium magneto-nanoparticles. Comp Bio Med 2016;78:29–41.
[30] Hayat T, Farooq S, Ahmad B, Alsaedi A. Homogeneous-heterogeneous reactions and heat source/sink effects in MHD peristaltic flow of micropolar fluid with Newtonian heating in a curved channel. J Mol Liq 2016;223:469–88.
[31] Hayat T, Tanveer A, Alsaedi A. Numerical analysis of partial slip on peristalsis of MHD Jeffery nanofluid in curved channel with porous space. J Mol Liq 2016;224:944–53.
[32] Ramzan M, Bilal M, Chung JD. Influence of homogeneous–heterogeneous reactions on MHD 3D Maxwell fluid flow with Cattaneo-Christov heat flux and convective boundary condition. J Mol Liq 2017;230:415–22.
[33] Hayat T, Asghar S, Tanveer A, Alsaedi A. Homogeneous–heterogeneous reactions in peristaltic flow of Prandtl fluid with thermal radiation. J Mol Liq 2017;240:504–13.
[34] Hayat T, Bibi A, Yasmin H, Ahmad B. Simultaneous effects of Hall current and homogeneous/heterogeneous reactions on peristalsis. J Taiwan Inst Chem Eng 2016;58:28–38.
[35] Javed M, Hayat T, Mustafa M, Ahmad B. Velocity and thermal slip effects on peristaltic motion of Walters-B fluid. Int J Heat Mass Transfer 2016;96:210–7.
[36] Tanveer A, Hayat T, Alsaedi A, Ahmad B. Mixed convective peristaltic flow of Sisko fluid in curved channel with homogeneous–heterogeneous reaction effects. J Mol Liq 2017;233:131–8.
[37] Hayat T, Aslam N, Alsaedi A, Rafiq M. Endoscopic effect in MHD peristaltic activity of hyperbolic tangent nanofluid: a numerical study. Int J Heat Mass Transfer 2017;115:1033–42.
[38] Hayat T, Rafiq M, Ahmad B. Influences of rotation and thermophoresis on MHD peristaltic transport of Jeffrey fluid with convective conditions and wall properties. J Magn Magn Mater 2016;410:89–99.
[39] Hayat T, Quratulain A, Alsaedi M Rafiq, Ahmed B. Joule heating and thermal radiation effects on peristalsis in curved configuration. Res Phys 2016;6:1088–95.
[40] Hayat T, Shafique M, Tanveer A, Alsaedi A. Slip and Joule heating effects on radiative peristaltic flow of hyperbolic tangent nanofluid. Int J Heat Mass Transfer 2017;112:559–67.